INTERNATIONAL JOURNAL OF COMPUTERS COMMUNICATIONS & CONTROL
Online ISSN 1841-9844, ISSN-L 1841-9836, Volume: 21, Issue: 5, Month: October, Year: 2026
Article Number: 7652, https://doi.org/10.15837/ijccc.2026.5.7652

CCC Publications

AGORA UNIVERSITY PRESS

Robust Integrated Control for Dual Active Bridge Converters in Aircraft Power System

Muhammad Arif Anwar, Wang Li Marius Balas, Jason Gu, Muhammmad Usman Asad, Ghulam Abbas, Umar Farooq

Muhammad Arif Anwar and Wang Li
Department of Electrical Engineering, College of Automation and Control
Nanjing University of Aeronautics and Astronautics, Nanjing, China
muhammadarif.anwar@outlook.com
liwang@nuaa.edu.cn

Marius Balas
Department of Automatics and Applied Software at the Faculty of Engineering,
University "Aurel Vlaicu" Arad, Romania
marius.balas@uav.ro

Ghulam Abbas
Department of Electrical
The University of Lahore, Pakistan
ghulam.abbas@ee.uol.edu.pk

Jason Gu, Muhammad Usman Asad and Umar Farooq
Department of Electrical and Computer Engineering
Dalhousie University Halifax, Canada
Jason.gu@dal.ca
muhammad.asad@dal.ca
umar.farooq@dal.ca

Abstract

This paper presents the design and implementation of a robust adaptive control strategy for a Dual Active Bridge (DAB) converter used in More Electric Aircraft (MEA) applications. In MEA electrical architectures, a 270 V DC main bus must reliably supply regulated 28 V DC power for onboard systems such as avionics and battery subsystems. In response to this demand, a new controller based on a Fractional-Order Adaptive Super-Twisting Algorithm (FO-ASTA) integrated with a Model Reference Adaptive Control (MRAC) framework is proposed. The controller enhanced the robustness and chattering-free properties of super-twisting sliding mode control, the dynamic memory effects of fractional-order systems, and the real-time adaptability of MRAC.The proposed FO-ASTA controller integrated with the MRAC scheme is evaluated under steady-state conditions, load variations, reference changes, and parametric uncertainties. Moreover, its performance is compared with the Fractional-Order Sliding Mode Controller (FOSMC) and Fractional-Order Super-Twisting Algorithm (FOSTA) controllers. Simulation results on the circuit level confirm that the proposed controller outperforms the alternatives in terms of tracking accuracy, convergence speed, disturbance rejection, and control smoothness. This makes it a strong candidate for high-performance DC–DC conversion in next-generation MEA power systems.

Keywords: Robust Control, DC - DC Converter, Aircraft DC Power System.

1 Introduction

Modern aircraft are evolving towards electrified systems through the More Electric Aircraft (MEA) model, replacing hydraulic and pneumatic subsystems with electrical counterparts. This transition significantly raises onboard electrical demands; however, it offers potential benefits, including higher efficiency, reduced maintenance costs, lighter overall weight, and reduced CO2 emissions. The electrical power system in MEA has developed considerably over time; however, the DC distribution power system is one of the most prospective power systems due to its cable saving potential with respect to three three-phase AC system [1] [2]. The DC power system utilized different voltage levels as in 270 HVDC and 28 VDC is adopted. The 270 HVDC bus powered the actuation, propulsion auxiliaries, and environmental systems. The 270 EPS is depicted in Figure 1 in which threes stage generator produced AC power, which is converted to DC ones with the help of an uncontrolled diode rectifier and powered the 270 V DC bus. The essential subsystems, such as avionics, lighting, and battery storage systems, operate at 28 V DC, which is referred to as low voltage (LVDC). This requires a robust, efficient, and reliable DC–DC converter to interface the two voltage levels [3],[4]. The loads are connected and disconnected with the bus through the solid-state controlled switches, and they are also used to maintain the connection between the different buses. The Dual Active Bridge (DAB) converter is widely adopted in aerospace power systems for this task due to its bidirectional power transfer, galvanic isolation, higher power density and potential for soft-switching operation [5][6]. These converters are also extensively used in other fields where reliable power conversion and isolation are crucial, including microgrids, renewable energy interfaces, and electric vehicle charging systems. The conventional control strategies such as PI controller [7], feed forward control [8], and PID with dead zone compensation [9] have been adopted due to its simple structure, straight forward tuning method and implementation. However, their performance significantly degraded in transient state and reference change conditions and system uncertainties. In [10][11], sliding mode controller (SMC), back stepping SMC for nonlinear system[12] and adaptive SMC are introduced for DAB converter to handle the uncertainties and to improve the dynamic response. Although the system performance and stability are improved with these controllers, they were accompanied by chattering effects and required careful gain tuning, which may become a critical problem while designing a controller for the DAB issue. Second-order SMC is capable of reducing chattering while maintaining good tracking accuracy and robustness [13]. But, implementing second-order sliding mode control requires calculating the first derivative of the sliding variable, introducing additional complexity into the control design.The fuzzy-based controllers presented in [14][15]

which is nonlinear controller and due to the fact that it has not required the system parameters through system modelling and it demands fewer assumptions regarding initial parameters. Nevertheless, it can enhance the system performance to some extent, but the design process is computationally complex due the involvement of membership function; moreover, performing stability analysis remains notably complex when using fuzzy-based methods.For the compensation of these issues, researchers also utilised the advanced control approach, including observer-based designs [16], [17] H-infinity control frameworks [18],[19] and mixed sensitivity-based H-infinity [20] controllers are investigated, especially when the parameters are uncertain in converters and in inverters, which improve the performance and stability of the system. However, the response of the system is slow with these controllers, and additionally, by the selection of the weighing function, it's become more challenging. In [21],[22] and in [23], adaptive methods such as MRAC and adaptive neural networks are adopted for DAB converter control. They provided notable improvements in performance and robustness, but they often imposed high computational costs or introduced new sensitivities to modelling errors and their response is often slow for transient conditions. In [24] the super twisting algorithm-based controller (STA)and RBFNN SMC [25] control are adopted to improve the system response; however, due to parameter tuning complexity, the system response is slow in the transient and overshoot is also high. In recent years, the Super Twisting Sliding Mode Controller (ST-SMC) [26] and third-order STA [27] have been applied to DAB converters to improve voltage regulation and system response. The performance of the designed controller is compared with SMC and PI controllers. Although it shows better performance, especially during transient conditions. However, the design in this work considered a narrow voltage transformation ratio, which limits its adaptability across wider operating ranges. Moreover,

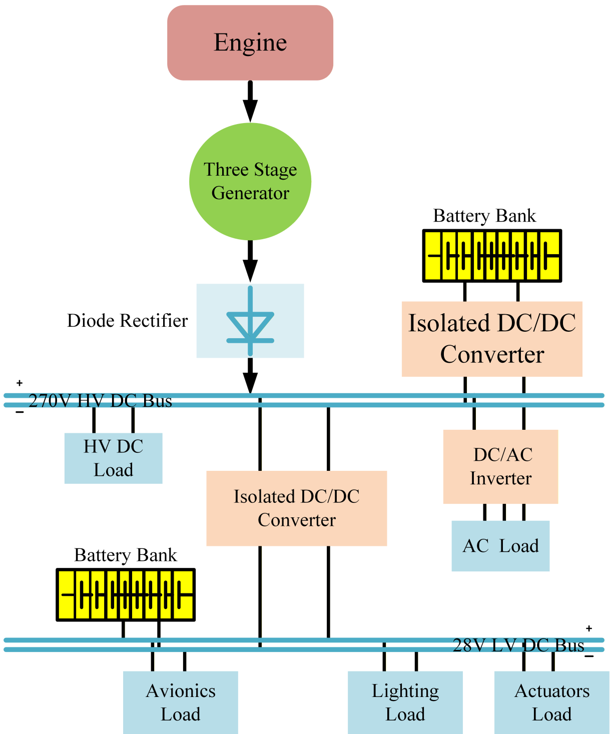

Figure 1: Aircraft DC Power System

implementing a DAB for 270 V to 28 V conversion presents specific challenges as its performance is highly sensitive to control strategy, particularly under wide load variation, parameter uncertainty, dynamic flight conditions, high switching frequency and high conversion ratio. The converter stability and robustness are important in industrial applications, especially for MEA power systems. A Fast transient response is preferable since a significant output voltage variance over an extended period of time might cause the system as a whole to become unstable. In order to provide a better control strategy, it is necessary to address the parameter uncertainty and mismatch, which also affect the converter's stability and operation.

Therefore, this study addresses this gap by presenting a hybrid controller that combines a model reference adaptive control (MRAC) scheme with a fractional-order adaptive super-twisting algorithm (FO-ASTA). Specifically designed to address the strict power regulation needs of MEA systems. The main contributions of this manuscript are as follows:

(1) An independent FOSMC is designed for the DAB converter based on a reduced-order model. The resulting control signal is passed through an integrator to ensure stable and robust operation under uncertain and nonlinear conditions.

(2) The FO-ASTA controller is designed and integrated with the MRAC scheme to form a unified control strategy. Its performance is comparatively evaluated against the robust FOSMC and FOSTA controllers under various operating conditions.

(3) A comprehensive stability and robustness analysis is conducted, validating the controller's capability to handle parametric uncertainties and load disturbances effectively.

(4) The controller performance is assessed under variable load conditions, input voltage fluctuations, and reference tracking changes, demonstrating improved dynamic response and disturbance rejection.

2 DAB Converter Topology and Modelling

The DAB converter configuration is depicted in Figure 2, which consists of two full H-bridge inverters: one connected to the primary side of the configuration and the other connected to the secondary side of the high-voltage transformer. The input voltage is denoted as V_{in}, while the output voltage on the secondary side is denoted as V_{out} and is connected to a low-voltage bus through an output capacitor C_{out}. The equivalent inductance L_k, includes the transformer's leakage inductance

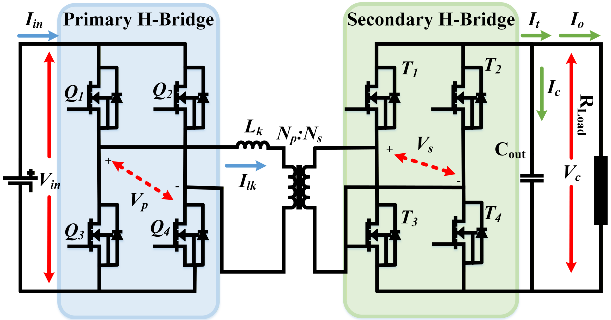

Figure 2: DAB Converter Topology

and any auxiliary inductance that supports power transfer. The load, represented by R_L, is connected to the secondary side of the transformer, and I_0 indicates the load current. The variable n represents the turns ratio of the transformer.

Table 1: Converter Parameters

Parameters	**Value**
Input voltageV_{in}	270 V
Output voltageV_o	28 V
Transformer voltage ratio N	10
Equivalent inductance L_k	4.9 mH
Power rating	1 kW
Switching frequency f_s	100 kHz
Output capacitor C	2.9 mF

The two symmetric H-bridges consist of semiconductor switches Q_{1-4} and T_{1-4}, located on the primary and secondary sides of the transformer. Figure 3 illustrates the high-frequency square-wave voltages on the primary and secondary sides of the transformer, labeled as V_p and V_s, using single-phase shift (SPS) modulation, along with the current waveform of the transformer in the DAB converter. The bidirectional DAB is designed to transfer high power efficiently between its terminals. The amount of power transmitted from the primary to the secondary bridge during each switching cycle can be expressed as:

$$P_s = \frac{V_{in}\,V_{out}}{2Nf_sL_k}\,d\,(1-|d|) \tag{1}$$

where N is the transformer turns ratio,f_s is the switching frequency, and d is the phase-shift ratio defined as $d = \delta/\pi$, with δ representing the angular phase shift between the two bridges. The phase-shift ratio, equivalent inductance, and switching frequency are the key parameters responsible for power transfer from the input port to the output port of the DAB converter, as expressed in (1).

Therefore, the secondary bridge's average output current during a single switching period can be represented as:

$$I_s = \frac{V_{in}}{2Nf_sL_k}\,d\,(1-|d|) \tag{2}$$

Assuming an ideal transformer and neglecting magnetizing currents, the reduced-order averaged model for the DAB converter by resolving the above two equations under SPS modulation is expressed.

$$\frac{dV_{out}}{dt} = \frac{V_{in}}{2Nf_sL_kC_{out}}\,\delta(1-|\delta|) - \frac{V_{out}}{RC_{out}} \tag{3}$$

This reduced-order model significantly simplifies the controller design process without compromising on accuracy, and the performance of the reduced-order model is better than the harmonic model, generalized average model and discrete time models [28]. Two distinct approaches are identified in the

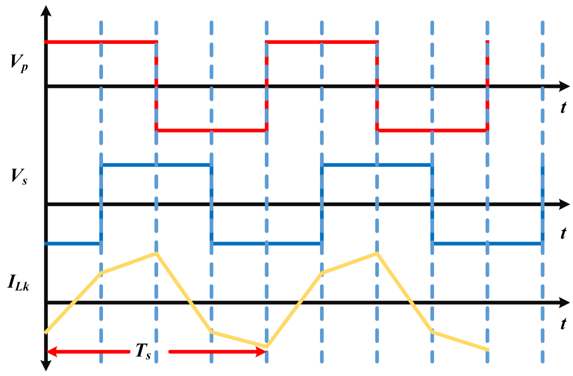

Figure 3: Bridge voltage and inductor current waveform for SPS modulation.

literature to achieve the control design: either the inversion of the function δ or linear approximations. An alternate strategy is adopted in this work that includes δ.

$$\delta = \int u\, dt \tag{4}$$

and its time derivative is given by:

$$\frac{d\delta}{dt} = u \tag{5}$$

In this scenario, the control objective is to drive the average of the output voltage at the LV bus to a desired value V_{ref} by acting on the control input u. , consequently, the system exhibits a relative degree of two. The DAB converter parameters are given in Table 1.

3 Controller Design

In this section, initially, an FO-SMC controller is formulated for the system described in Eq. (3) to ensure robust voltage regulation and disturbance rejection. The design of the FO-SMC establishes the foundation for the proposed integrated strategy by defining the fractional sliding surface and its associated control law, which guarantee finite-time convergence of the tracking error and robustness against model uncertainties. Afterwards, the proposed controller is developed, combining the FO-ASTA with the MRAC structure, and the combined control law is also constructed. Moreover, a comprehensive stability analysis based on Lyapunov theory is also presented for both the FO-ASTA and MRAC components, and for the overall hybrid controller, ensuring finite-time convergence, boundedness of all internal states, and asymptotic voltage tracking under practical operating conditions

3.1 Fractional order sliding mode controller design

The controller objective is to regulate the output voltage V_{out} at the LV bus to a desired value by acting on the control input u. The voltage tracking error is defined as

$$e(t) = V_{ref} - V_{out}(t) \tag{6}$$

The fractional sliding surface is defined in eq (7) for FOSMC

$$S(t) = \lambda_1 e(t) + \lambda_2 D^{-\alpha} e(t) \tag{7}$$

Whereλ_1 and λ_2 are the tuning parameters and $D^{-\alpha}$ denotes the Riemann-Liouville fractional integral operator The fractional order $\alpha = 0.6$ was optimized for this application. By taking the derivative of $S(t)$ with dynamic extension and putting the dynamics of the system

$$\dot{S}(t) = -\lambda_1 \left(\frac{V_{in}}{2NfsL_kC_{out}} \delta \left(1 - \frac{|\delta|}{\pi}\right) - \frac{V_{out}}{RC_{out}} \right) \qquad + \lambda_2 D^{1-\alpha} e(t) + \gamma u \tag{8}$$

The control law is designed as

$$u_{\text{FOSMC}} = -K_{\text{FOSMC}}\, \text{sign}(S(t)) \tag{9}$$

Where K_{FOSMC} is the controller gain with $K_{\text{FOSMC}} > 0$. The controller configuration is represented in Figure 4 with the sliding surface. For the stability of the system, the reachability condition must hold:

$$S(t)\, \dot{S}(t) < 0 \tag{10}$$

$$S\dot{S} = S\left[\phi - \gamma K_{\text{FOSMC}}\, \text{sign}(S)\right] \leq |S|(|\phi| - \gamma K_{\text{FOSMC}}), \tag{11}$$

where

$$\phi = -\lambda_1 \left(\frac{V_{in}\, \delta \left(1 - \frac{|\delta|}{\pi}\right)}{2N f_s L_k C_{out} \pi} - \frac{V_{out}}{R_L C_{out}} \right) + \lambda_2 D^{\,1-\alpha} e(t) \tag{12}$$

here

$$\gamma = \frac{\lambda_1 V_{in}\, (\pi - 2|\delta|)}{2N f_s L_k C_{out} \pi} \tag{13}$$

For stability, the controller gain must satisfy $K_{\text{FOSMC}} > \dfrac{|\phi|\text{max}}{\gamma\text{min}}$, ensuring that the sliding condition $S(t)\dot{S}(t) < 0$ is achieved.

3.2 Proposed integrated controller

In this section, the proposed hybrid controller is developed. The design begins with the formulation of the FO-ASTA controller, followed by its integration with the MRAC scheme.The complete controller architecture is depicted in Figure 5. In which the FO-ASTA controller works based on a fractional-order sliding surface, which is constructed using the tracking error $e = r - V_{\text{dc}}$. This switching surface further feeds into the adaptive mechanism that adjusts the super twisting gain in real time, enabling the controller to respond effectively to varying operating conditions without requiring manual tuning. This super-twisting algorithm generates the controller output signal $u_{\text{FO-ASTA}}$. In parallel, the MRAC framework processes the same desired reference signal r. This reference voltage r is applied both to the reference model and the main controller. The reference model generates an ideal output trajectory, denoted Y_{m}, which is compared with the system output V_{dc} and the error e_r signal is generated, which is further processed through dead zone compensation and with an adaptive law. This enhances the overall robustness of the MRAC loop, particularly in high-frequency switching systems like DAB converters. An adaptive law continuously updates the controller parameters based on the error between the converter output and the model output. The controller within the MRAC configuration generates the controller signal u_{MRAC}. The combined control signal from the FO-ASTA and MRAC controller regulates the phase shift that determines power transfer through the DAB converter

The control law of the FOASTA controller is given as:

$$u_{Fo-ASTA} = -k_1(t)\, |S|^{1/2}\, \text{sign}(S) + \nu, \tag{14}$$

with the auxiliary dynamics

$$\dot{\nu} = -k_2(t)\, \text{sign}(S), \tag{15}$$

The k_1 and k_2 represent the FO-ASTA gain and the k_1 is generally responsible for improving the system dynamics response and reducing the chattering phenomena, the gain k_2 improves the system steady state response. The selection of k_1,k_2 determines the sliding surface S reaches the zero in finite time in the presence of disturbance and parameter variations. An adaptive gain mechanism is incorporated to enhance adaptability and eliminate the need for fixed, large gains, enabling k_1,k_2 to vary in real time in response to the magnitude of the sliding variable. Where the adaptive gains mechanism is given by

$$k_i(t) = k_{i,\min} + (k_{i,\max} - k_{i,\min})\tanh(\beta|S(t)|)\,, \quad i = 1, 2, \tag{16}$$

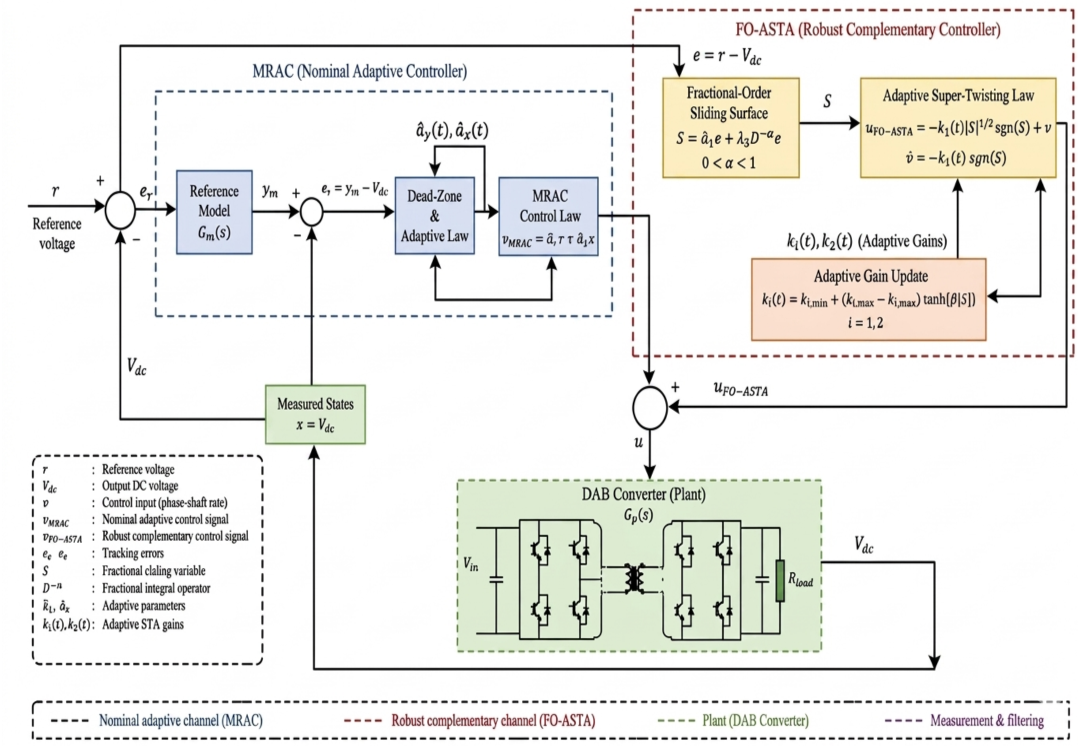

Figure 4: Proposed Controller Structure.

Table 2: Control Parameters for Different Methods

Control Method	**Parameter**	**Value**
FOSMC	K_1	0.95
	K_2	1.2×10^4
	K_{FOSMC}	45
FOSTA	λ_1	1×10^{-2}
	λ_2	5×10^{-6}
	K_1	220
	K_2	120
FOASTA	λ_1	1×10^{-2}
	λ_2	5×10^{-6}
	K_1 (min–max)	180–250
	K_2 (min–max)	100–140
MRAC	γ_1	0.94
	γ_2	0.85

for design constants $k_{i,\min}, k_{i,\max}, \beta > 0$. The parameter β governs the rate at which the adaptive gain $k_i(t)$ changes from its minimum value $k_{i,\min}$ to its maximum value $k_{i,\max}$, thereby controlling the responsiveness of the adaptation process. The $\tanh(\cdot)$ function establishes a smooth, nonlinear mapping that, depending on the size of the sliding variable, continually modulates the controller gain within these predetermined limits, guaranteeing quick adaptation without adding discontinuities to the control signal The switching function $S(t)$ and its derivative $\dot{S}(t)$ are defined as in (7) and (8), respectively.

The MRAC controller is designed to regulate the output voltage V_{out} to the desired reference V_{ref}. The reduced-order plant model is defined as

$$\dot{x} = -a_p x + b_p u, \tag{17}$$

where $x = V_{out}$ and $a_p, b_p > 0$ are unknown parameters. The reference model is defined as

$$\dot{y}_m = -a_m y_m + b_m r(t), \quad e_r = x - y_m, \tag{18}$$

where y_m is the model output, $r(t)$ is the reference input, and e_r is the tracking error.

The MRAC control law is

$$u(t)_{MRAC} = a_r(t)r(t) + a_x(t)x(t), \tag{19}$$

with adaptation laws (including dead-zone compensation)

$$\dot{a}_r(t) = \begin{cases} -\mu\, e_r(t)\, r(t), & |e_r(t)| > e_{dz}, \\ 0, & |e_r(t)| \leq e_{dz}, \end{cases} \tag{20}$$

$$\dot{a}_x(t) = \begin{cases} -\mu\, e_r(t)\, x(t), & |e_r(t)| > e_{dz}, \\ 0, & |e_r(t)| \leq e_{dz}, \end{cases} \tag{21}$$

where $\mu > 0$ is the adaptation gain and e_{dz} is the dead-zone threshold. The proposed controller integrates the FO-ASTA dynamics (14)–(16) with the MRAC structure (19)–(21). The resulting scheme inherits the robustness and finite-time convergence of FO-ASTA while maintaining the adaptability and tracking properties of MRAC

The complete control input u is constructed by adding the FO-ASTA and MRAC contributions which is defined as

$$\begin{aligned} u &= u_{\text{FO-ASTA}} + u_{\text{MRAC}} \\ &= \left[-k_1(t)\,|S|^{1/2}\,\text{sgn}(S) + \nu\right] \\ &\quad + \left[a_r(t)\,r(t) + a_x(t)\,x(t)\right]. \end{aligned} \tag{22}$$

While MRAC adjusts the nominal control for parameter uncertainties, the FO-ASTA acts on the sliding surface $S(t)$, which includes fractional dynamics for improved transient performance.

3.3 Stability Analysis

For the stability of the proposed controller, we analyze both the FO-ASTA and MRAC components. For the FO-ASTA part, consider the Lyapunov function

$$V_1(S, \nu) = \frac{1}{2}S^2 + \frac{1}{2}\gamma\nu^2. \tag{23}$$

$$\dot{V}_1 = S\,\dot{S} + \gamma\,\nu\,\dot{\nu}. \tag{24}$$

Its derivative along the trajectories of the closed-loop system is

$$\dot{V}_1 = S\phi - \gamma k_1(t)|S|^{3/2} + \gamma S\nu - k_2(t)|\nu|, \tag{25}$$

where ϕ is as defined in (12). The cross-term $\gamma S\nu$ is bounded by Young's inequality:

$$|\gamma S\nu| \leq \frac{\gamma\varepsilon}{2}S^2 + \frac{\gamma}{2\varepsilon}\nu^2, \qquad \forall\, \varepsilon > 0. \tag{26}$$

Thus,

$$\dot{V}_1 \leq |S|\,|\phi| - \gamma\,k_1(t)\,|S|^{3/2} + \gamma\,\epsilon\,\frac{S^2}{2} + \frac{\gamma}{2\epsilon}\,\nu^2 - \gamma\,k_2(t)\,|\nu|. \tag{27}$$

To ensure $\dot{V}_1 < 0$, the adaptive gains are selected such that

$$k_1(t) > \frac{|\phi|_{\max}}{\gamma|S|^{1/2}} + \frac{\varepsilon}{2}|S|^{1/2}, k_2(t) \qquad > \frac{\gamma}{2\varepsilon}|\nu|. \tag{28}$$

The tanh based adaptation ensures that $k_1(t)$ and $k_2(t)$ increase with $|S|$, while remaining bounded between $k_{i,\min}$ and $k_{i,\max}$. Under these conditions, the derivative of the Lyapunov function satisfies

$$\dot{V}_1 < -\eta V_1^{1/2}, \quad \eta > 0. \tag{29}$$

Thus, the reachability condition

$$S\dot{S} = S(\phi - \gamma k_1 |S|^{1/2}\mathrm{sign}(S) + \gamma\nu) < 0 \tag{30}$$

is satisfied, guaranteeing finite-time convergence of S to zero and robustness against uncertainties.

For the MRAC part, consider the Lyapunov function

$$V_2 = \frac{1}{2}e_r^2 + \frac{1}{2}\mu(\tilde{a}_r^2 + \tilde{a}_x^2), \tag{31}$$

where $\tilde{a}_r = a_r - a_r^*$ and $\tilde{a}_x = a_x - a_x^*$ are parameter errors. When $|e_r|> e_{dz}$, its derivative is

$$\dot{V}_2 = e_r\,\dot{e}_r + \frac{1}{\mu}(\tilde{a}_r\dot{\tilde{a}}_r + \tilde{a}_x\dot{\tilde{a}}_x), \tag{32}$$

and substituting the plant dynamics and adaptation laws gives

$$\dot{V}_2 = -a_m e_r^2 \leq 0. \tag{33}$$

When $|e_r|\leq e_{dz}$, the adaptation is frozen ($\dot{a}_r = \dot{a}_x = 0$), and the same inequality holds:

$$\dot{V}_2 = -a_m e_r^2 \leq 0. \tag{34}$$

Hence, by Barbalat's lemma, $e_r(t) \to 0$ in the absence of a dead zone, while with a dead zone the tracking error is uniformly ultimately bounded and parameter drift is eliminated.

Finally, consider the composite Lyapunov function for the hybrid controller:

$$V_h = V_1 + V_2. \tag{35}$$

$$V_h = \frac{1}{2}S^2 + \frac{1}{2}\gamma\nu^2 + \frac{1}{2}e_r^2 + \frac{1}{2\mu}\left(\tilde{a}_r^2 + \tilde{a}_x^2\right). \tag{36}$$

Since $\dot{V}_1 \leq 0$ under the gain conditions (25)–(26), and $\dot{V}_2 \leq 0$ as shown in (30)–(31), the overall derivative satisfies

$$\dot{V}_h = \dot{V}_1 + \dot{V}_2 \leq 0. \tag{37}$$

Thus, all closed-loop signals remain bounded, the sliding variable converges in finite time, and the tracking error is ultimately bounded. The proposed FO-ASTA–MRAC hybrid controller, therefore, ensures robust output tracking and stability in the presence of parameter variations and disturbances. The designed controller parameters are provided in Table 2. The implementation procedure of the proposed controller is summarised in Algorithm 1.

4 Simulation Results and Discussion

This section presents a comprehensive performance evaluation of the proposed integrated control structure with the FOSMC and FOSTA controllers .The simulations are conducted in MATLAB/Simulink for the FOSMC, FOSTA, and the proposed hybrid control approach. The performance of the proposed controller is evaluated against the FOSMC and FOSTA under various operating scenarios, including steady-state conditions, variable load, reference changes, reference variation with load change, and input voltage disturbances for the DAB converter. Furthermore, the controller performance is also observed under parameter uncertainty, as such uncertainties play a crucial role in the overall system stability and may drive the system toward instability if not properly addressed. The results are compared with the conventional FOSMC and FOSTA controllers to illustrate the superiority of the proposed control strategy in terms of faster transient recovery, reduced voltage deviation, and

Algorithm 1 Integrated FO-ASTA–MRAC Control Algorithm for DAB Converter

Require: Reference voltage r, measured output voltage V_{dc}, controller parameters $\lambda_1, \lambda_2, \alpha, \mu, k_{i,\min}, k_{i,\max}, \beta$

Ensure: Robust voltage regulation, adaptive tracking, finite-time convergence, and disturbance rejection

Define tracking error:
$e(t) = r(t) - V_{dc}(t)$
Construct fractional-order sliding surface:
$S(t) = \lambda_1 e(t) + \lambda_2 D^{-\alpha} e(t)$
Initialize adaptive gains:
$k_i(t) = k_{i,\min}, \quad i = 1, 2$
for each sampling instant t_k **do**
  Measure converter output voltage $V_{dc}(t_k)$
  Compute reference model output:
  $\dot{y}_m = -a_m y_m + b_m r$
  Compute MRAC tracking error:
  $e_r(t_k) = y_m(t_k) - V_{dc}(t_k)$
  if $|e_r(t_k)| > e_{dz}$ **then**
    Update adaptive parameters:
    $\dot{a}_r = -\mu e_r r$
    $\dot{a}_x = -\mu e_r x$
  else
    Freeze adaptation law:
    $\dot{a}_r = 0, \quad \dot{a}_x = 0$
  end if
  Compute MRAC control signal:
  $u_{MRAC} = a_r(t_k) r(t_k) + a_x(t_k) x(t_k)$
  Update adaptive super-twisting gains:
  $k_i(t_k) = k_{i,\min} + (k_{i,\max} - k_{i,\min}) \tanh(\beta |S(t_k)|)$
  Compute FO-ASTA control law:
  $u_{FO\text{-}ASTA} = -k_1(t_k) |S(t_k)|^{1/2} \mathrm{sgn}(S(t_k)) + \nu(t_k)$
  Update auxiliary dynamics:
  $\dot{\nu}(t_k) = -k_2(t_k) \mathrm{sgn}(S(t_k))$
  Construct final control input:
  $u(t_k) = u_{MRAC}(t_k) + u_{FO\text{-}ASTA}(t_k)$
  Apply control signal $u(t_k)$ to the DAB converter
  Update converter dynamics:
  $\dot{V}_{dc} = \frac{V_{in}}{2N f_s L_k C_o} \delta(1 - |\delta|) - \frac{V_{dc}}{RC_o}$
end for
Verify finite-time convergence:
$\dot{V}_1 < -\eta_1 V_1^{1/2}$
Verify MRAC stability:
$\dot{V}_2 = -a_m e_r^2 \leq 0$
Conclude overall stability:
$\dot{V} = \dot{V}_1 + \dot{V}_2 < 0$

improved steady-state accuracy. Under steady-state conditions, the converter operates at constant load and input voltage, allowing the evaluation of each controller's ability to maintain a stable output without external disturbances. As shown in Figure 5, the proposed integrated controller demonstrates significantly superior performance compared to the FOSMC and FOSTA controllers.It reaches the desired output voltage of 28 V within 10 ms, with a minor undershoot of 1.8 V. In comparison, the FOSMC and FOSTA controllers achieve a steady state at approximately 30 ms.

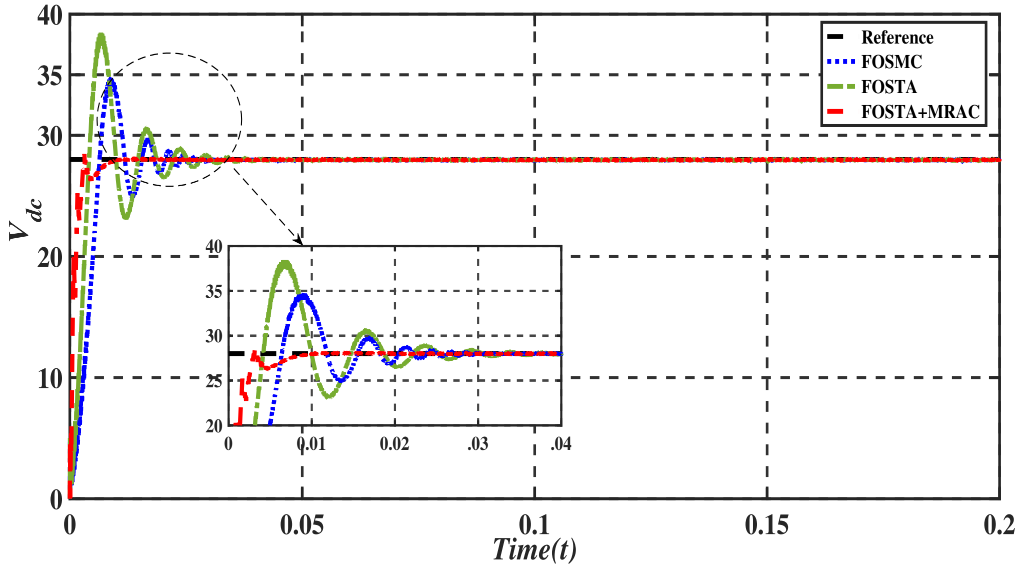

Figure 5: Output voltage under steady state condition with 270 V input voltage.

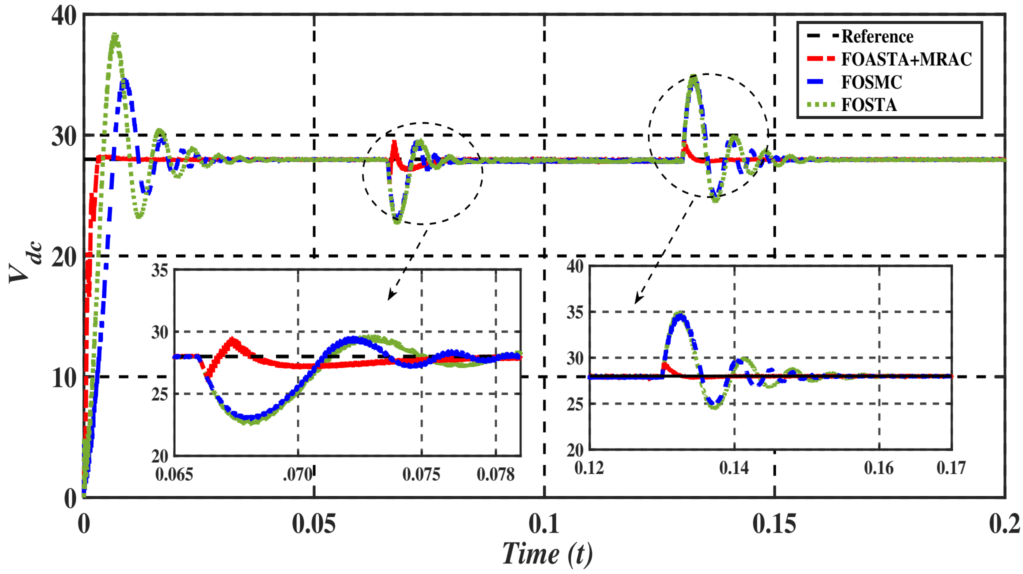

Figure 6: Output voltage under load change with 270 V input voltage.

The FOSMC exhibits an overshoot of up to 35 V and an undershoot of 3.2 V, while the FOSTA shows an even larger overshoot of 38 V and an undershoot of 5 V. However, all the designed controllers can accurately track the reference voltage at steady-state; however, the integrated controller performance is much superior than as compared to the FOSMC and FOSTA controllers.

Figure 6 illustrates the variable load condition, where at $t = 0.066$ s the load ($R_L = 1.57$ ohm) is added to the system. The FOSMC and FOSTA controllers both exhibit an undershoot of up to 5.4 V and an overshoot of 1.4 V, converging to the steady-state value in approximately 19 ms and 21 ms, respectively. In contrast, the proposed controller illustrates the smaller

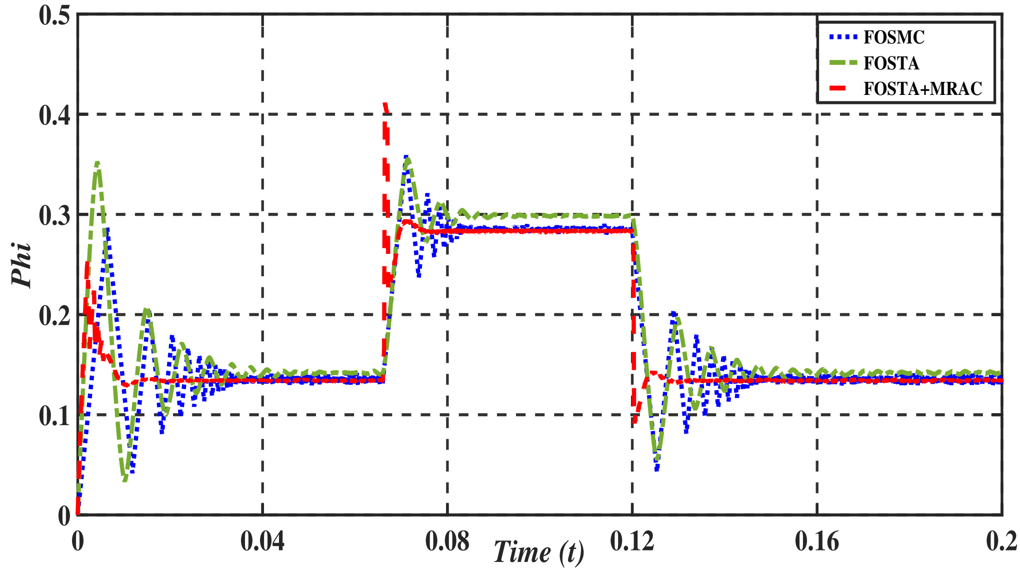

Figure 7: Phase shift under variable load condition.

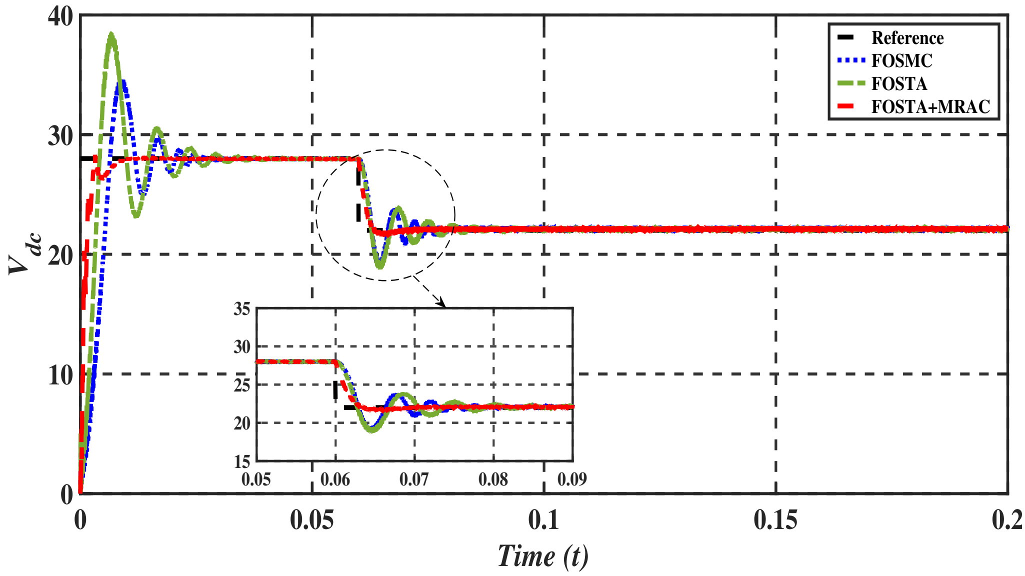

Figure 8: System response with reference change

undershoot of 2.1 V and overshoot up to 1.4 V and converges to a steady state value in 10 ms. For the detached load condition that occurred at time 0.13 sec the FOSMC shows the overshoot of 6.4 V and undershoot up to 3 V and settled down in 21ms, the FOSTA controller shows the overshoot of 7 V, undershoot up to 3.6 V and achieved the nominal bus voltage in 25 ms. Whereas the hybrid proposed controller converges to the steady state in 1.3 ms with overshoot of 1.2 V with no undershoot. This shows that the designed controllers are robust against the load changing disturbance and track the desired voltage reference nicely. However, the performance of the proposed controller is much better than the FOSMC and FOASTA in terms of fast transient response with low voltage variations.
Figure 7 demonstrates the control signal phase shift under variable load conditions for the FOSMC, FOASTA, and the proposed controller.The load variation occur at t=.066 sec and t=.012 sec. The FOSMC exhibits high-frequency chattering and slower convergence, FOASTA reduces chattering but still suffers from mild oscillations. The proposed integrated controller demonstrates superior performance, with the smoothest output, minimal overshoot, and fast settling time. This validates its effectiveness in reducing chattering, in enhancing robustness and tracking accuracy under load disturbances,making it highly suitable for practical DAB converters.

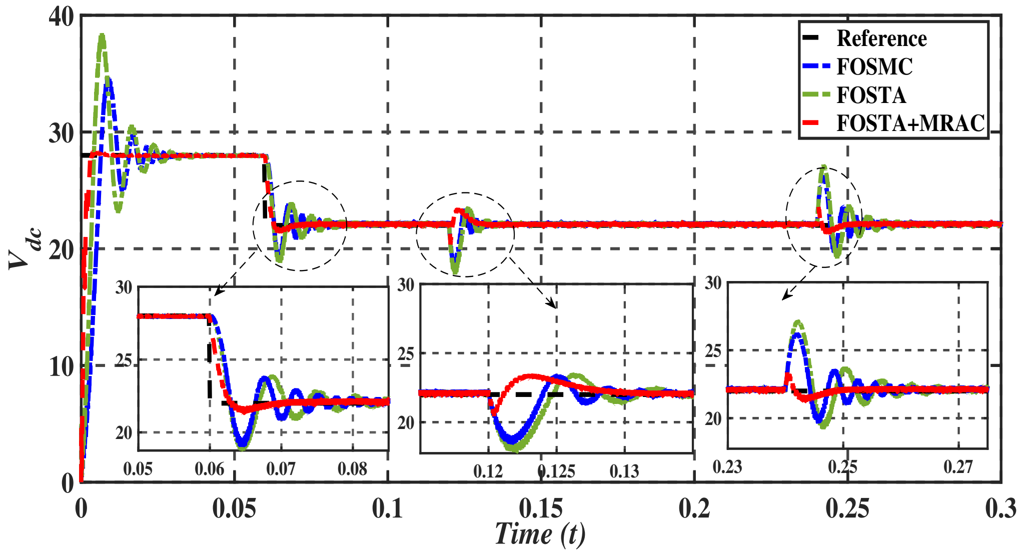

Figure 9: Output voltage with variable reference and load change

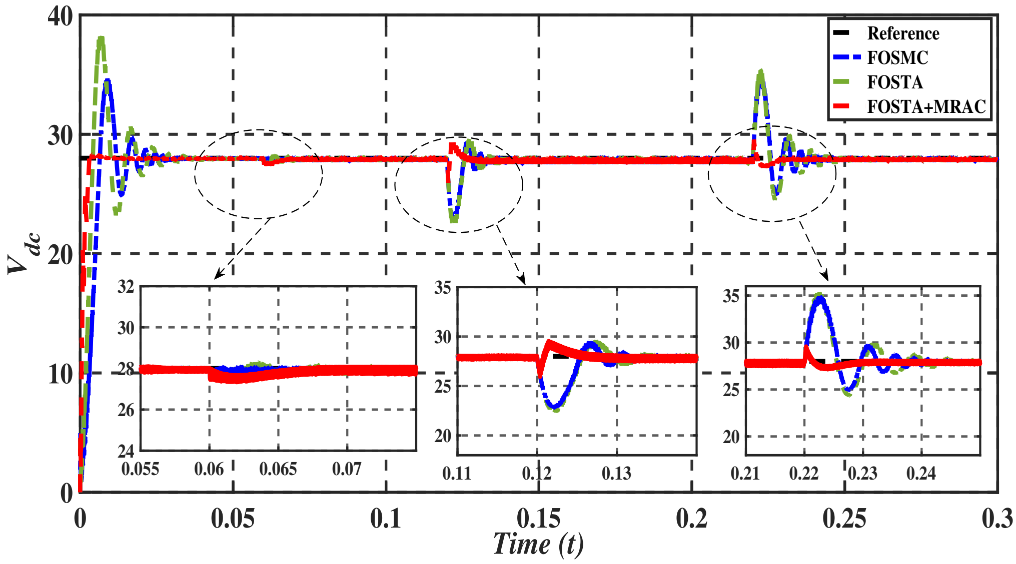

Figure 10: Output voltage under load change with 250 V input voltage

The controller's performance is also investigated under reference change conditions in Figure 8. The result illustrates that the designed controllers perfectly track the sudden reference change of 22 V, which occurs at time .06 sec. The proposed controller tracks the reference very quickly and reaches the steady state in 2 ms with the overshoot of only 0.6 V with no undershoot, while the FOSMC shows the undershoot of 3.3 V and overshoot up to 1.2 V, and FOSTA shows the 3.3 V undershoot and 1.8 V overshoot. Both controllers attained the desired referenced change value in 20 ms.
Figure 9 presents the variable load scenario combined with a reference change to 22 V. At $t = 0.12$ s, the load is attached to the system, and the proposed controller achieves the steady-state value within 9 ms, with an undershoot of 1.7 V and an overshoot of 1.4 V with less oscillations. The FOSMC and FOSTA controllers reach steady state after approximately 20 ms, showing overshoot of 1.4 V and undershoot up to 4.2 V.

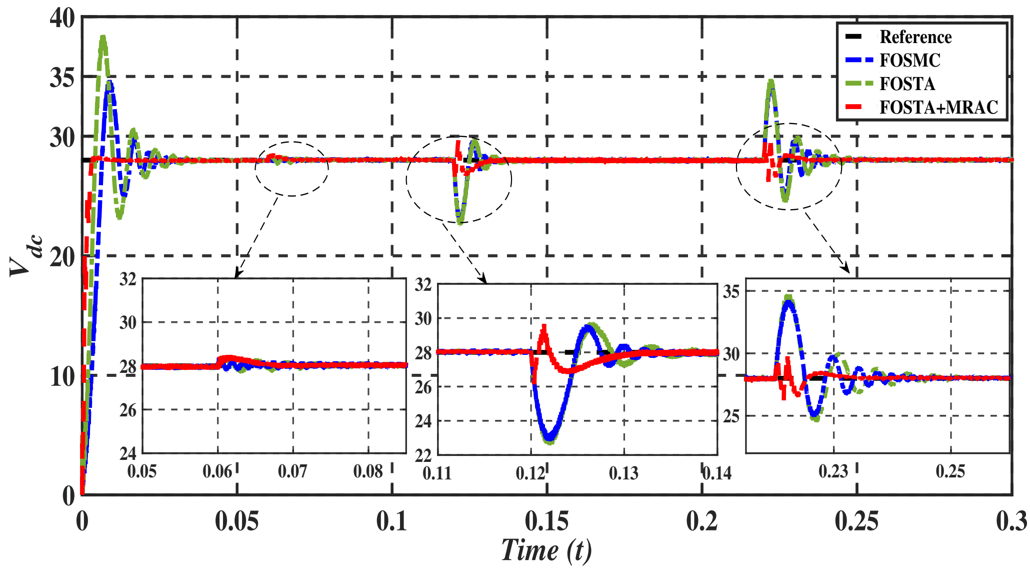

Figure 11: Output voltage under load change with 290 V input voltage

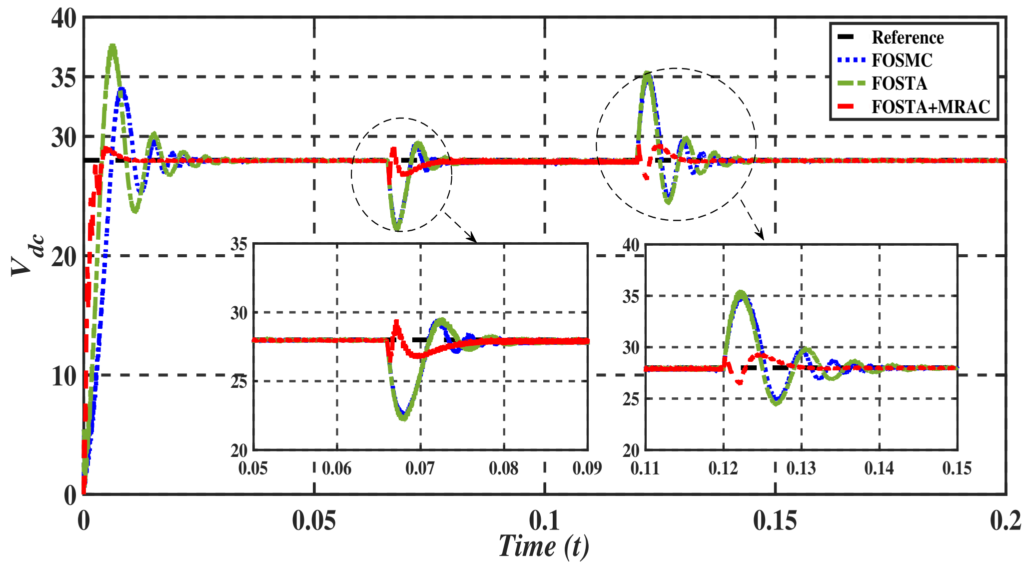

Figure 12: Output voltage with −15% change in capacitance

When the load is disconnected at $t = 0.24$ s, the proposed hybrid controller achieves the desired voltage in 10 ms with a small overshoot of 1.6 V. In comparison, the FOSMC and FOSTA controllers settle in 27 ms, exhibiting overshoots of 5 V and 4 V, respectively. These results under reference change conditions further confirm the superior performance of the proposed controller in achieving faster dynamic response and reduced voltage variations compared to the other two controllers.
Moreover, the controller implementation is also evaluated under sudden input voltage changes from 270 V to 250 V and 290 V at $t = 0.06$ s with varying load conditions, as shown in Figures 10 and 11, respectively. All the designed controllers exhibit robustness against input voltage variations and quickly recover the output voltage. During load connection and disconnection, the FOSMC and FOSTA controllers show similar behaviour with an input of 250 V, both controllers display a voltage deviation of 5.6 V and a settling time of 20 ms with noticeable oscillations. In contrast, the proposed hybrid controller demonstrates higher robustness, showing only a 2 V voltage dip and achieving voltage recovery within 10 ms. In the load-detached condition, the performance of the FOSMC

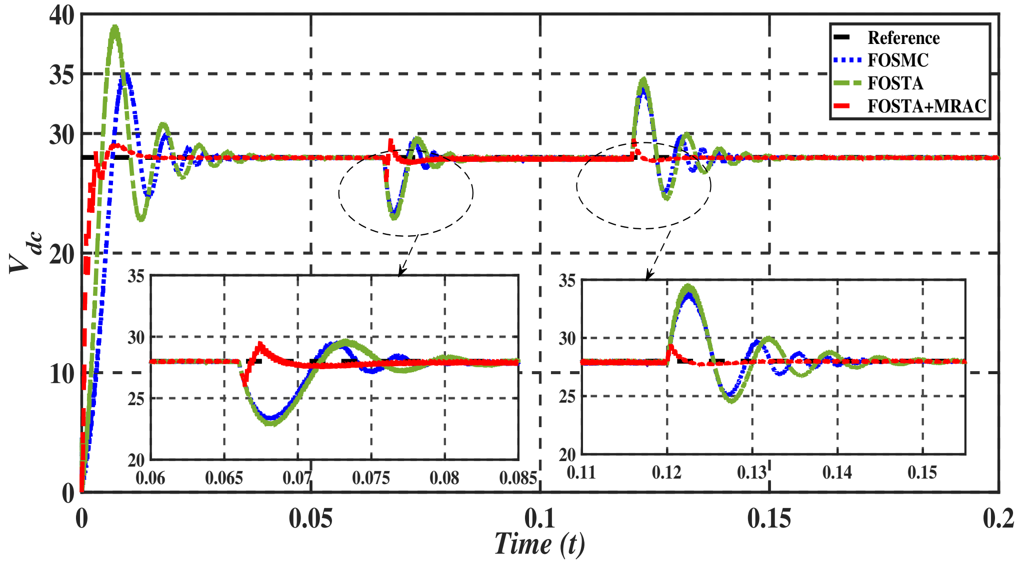

Figure 13: Output voltage with +15% change in capacitance

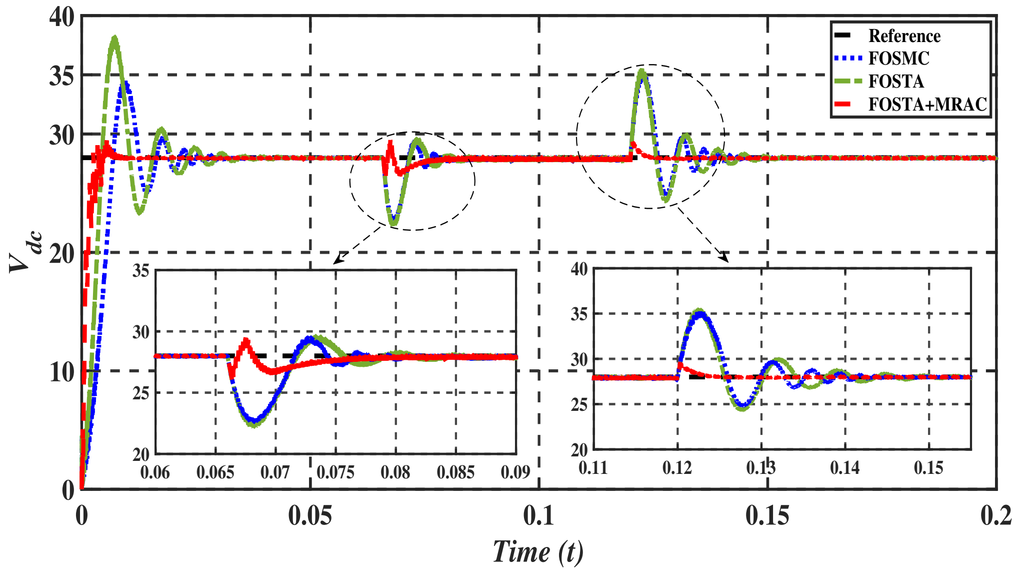

Figure 14: Output voltage with +10% change in Inductance

and FOSTA controllers degrade, exhibiting overshoot and undershoot of 7 V and 3 V, respectively, and reaching the steady-state voltage in 22 ms. The proposed integrated controller, however, shows only a 1.4 V overshoot with a smooth voltage response, attaining the reference voltage in 5 ms. For an input voltage of 290 V under load-attached conditions, the proposed controller achieves an undershoot and overshoot of 1.4 V with a settling time of 11 ms, whereas the other two controllers show an undershoot of 5.2 V and reach steady-state with oscillations in 16 ms. In the load-detached case, the FOSMC and FOSTA controllers exhibit voltage deviations of 7.2 V and 3.6 V, respectively, achieving the desired voltage in 24 ms with oscillations, while the hybrid controller settles smoothly within 9 ms with a minor overshoot of 1.4 V. Overall, when the input voltage varies from 250 V to 290 V under load-changing conditions, the proposed controller exhibits greater robustness and faster convergence to the desired voltage compared to the FOSMC and FOSTA controllers.

To examine robustness under parameter uncertainties, mismatches in capacitance and inductance values are introduced during controller implementation. Since the output capacitance and inductance significantly affect converter performance, ±15% variation in capacitance and 10% increase in inductance are considered from their nominal values. Figure 12 shows the controller responses for a −15% change in capacitance under variable load conditions. The proposed hybrid controller attains the desired output voltage with an under/overshoot of 1.6 V and converge to the desired state in 5 ms under load-attached conditions. In comparison, the FOSMC and FOSTA both controllers exhibit an undershoot of 5.9 V and an overshoot of 1.4 V, and take 10 ms to converge to the desired value. In the load-detached case, both FOSMC and FOSTA controllers show an overshoot of 7.5 V and reach steady-state within 20 ms, whereas the proposed controller achieves voltage recovery within 11 ms with only a 1.5 V voltage dip. Figure 13 presents the controller performance for a +15% change in capacitance. The proposed controller reaches steady-state within 4 ms with an undershoot of 2.1 V and an overshoot of 1.5 V. In contrast, the FOSMC and FOSTA controllers achieve voltage regulation in 14 ms with undershoots of 5.2 V and 4.8 V, and overshoots of 1.4 V and 1.6 V, respectively, under load-attached conditions at $t = 0.066$ s. Under load-detached conditions, the FOSTA and FOSMC controllers exhibit overshoots of 6.6 V and 5.6 V and settle within 27 ms, whereas the proposed controller converges to the nominal bus voltage in just 2 ms with a 1.5 V overshoot. Figure 14 illustrates the controller performance under a 10% inductance mismatch with load variations. In this case, the proposed hybrid controller achieves the desired output voltage with only a 1.6 V dip and settles within 12 ms under load-attached conditions. In comparison, the FOSMC and FOSTA controllers show voltage dips of 5.1 V and 5.8 V, respectively, reaching steady-state in 14 ms. For the load-detached condition, the hybrid controller achieves stable operation within 2 ms with a minor overshoot of 1.5 V, while the other two controllers settle within 25 ms, showing larger overshoots of approximately 7.2 V.

5 Conclusion

In this work, the integrated structure of FO-ASTA with MRAC has been proposed to govern the output voltage of DAB converter for MEA applications. The proposed controller provides the robust control and enhances the voltage regulation. A reduced-order model of the DAB converter has been employed to simplify the controller design and reduce computational complexity. The performance of the proposed controller is validated through comparison with the FOSMC and FOSAT controllers under different loading conditions, input voltage change and reference change conditions. The results demonstrate that the proposed robust controller achieves superior fast transient and steady-state performance, significantly improving the tracking accuracy and maintaining a stable output voltage even under large reference variations and with parameter uncertainty. The proposed control strategy for the DAB converter exhibits high robustness, improved dynamic behaviour, and enhanced steady-state voltage regulation, making it a promising solution for MEA power systems and battery energy storage applications.

Acknowledgements

The author is very thankful to the Chinese Government Scholarship (CSC) for supporting this research work at Nanjing University of Aeronautics and Astronautics, China.

Author contributions

The authors contributed equally to this work.

Conflict of interest

The authors declare no conflict of interest.

References

[1] Buticchi, G., Wheeler, P. and Boroyevich, D., 2022. The more-electric aircraft and beyond. Proceedings of the IEEE, 111(4), pp.356-370.

[2] Ni, K., Liu, Y., Mei, Z., Wu, T., Hu, Y., Wen, H. and Wang, Y., 2019. Electrical and electronic technologies in more-electric aircraft: A review. IEEE Access, 7, pp.76145-76166.

[3] Swaminathan, N. and Cao, Y., 2020. An overview of high-conversion high-voltage DC–DC converters for electrified aviation power distribution system. IEEE Transactions on Transportation Electrification, 6(4), pp.1740-1754.

[4] Karanayil, B., Ciobotaru, M. and Agelidis, V.G., 2016. Power flow management of isolated multiport converter for more electric aircraft. IEEE Transactions on Power Electronics, 32(7), pp.5850-5861.

[5] Keshmiri, N., Hassan, M.I., Rodriguez, R. and Emadi, A., 2021. Comparison of isolated bidirectional DC/DC converters using WBG devices for more electric aircraft. IEEE Open Journal of the Industrial Electronics Society, 2, pp.184-198.

[6] Tan, N.M.L., Abe, T. and Akagi, H., 2011. Design and performance of a bidirectional isolated DC–DC converter for a battery energy storage system. IEEE Transactions on Power Electronics, 27(3), pp.1237-1248.

[7] Qin, H. and Kimball, J.W., 2013. Closed-loop control of DC–DC dual-active-bridge converters driving single-phase inverters. ieee transactions on power electronics, 29(2), pp.1006-1017.

[8] Zhao, W., Zhang, X., Gao, S. and Ma, M., 2020. Improved model-based phase-shift control for fast dynamic response of dual-active-bridge DC/DC converters. IEEE Journal of Emerging and Selected Topics in Power Electronics, 9(1), pp.223-231.

[9] Segaran, D., Holmes, D.G. and McGrath, B.P., 2012. Enhanced load step response for a bidirectional DC–DC converter. IEEE Transactions on Power Electronics, 28(1), pp.371-379.

[10] Jeung, Y.C. and Lee, D.C., 2018. Voltage and current regulations of bidirectional isolated dual-active-bridge DC–DC converters based on a double-integral sliding mode control. IEEE Transactions on Power Electronics, 34(7), pp.6937-6946.

[11] Jeung, Y.C. and Lee, D.C., 2017, March. Sliding mode control of bi-directional dual active bridge DC/DC converters for battery energy storage systems. In 2017 IEEE applied power electronics conference and exposition (APEC) (pp. 3385-3390). IEEE.

[12] Ezzara, A., Ouadine, A.Y. and Ayad, H., 2025. Adaptive backstepping sliding mode fault-tolerant control of quadrotor UAV in the presence of external disturbances, uncertainties, and simultaneous actuator and sensor faults. International Journal of Computers Communications and Control, 20(5).

[13] Levant, A., 2003. Higher-order sliding modes, differentiation and output-feedback control. International journal of Control, 76(9-10), pp.924-941.

[14] Szeidert, I., Filip, I., Vasar, C. and Bordeasu, D., 2025. Comparative studies on the excitation control of a doubly fed induction generator using fuzzy PI controllers and classical PI/PID controllers. International Journal of Computers Communications and Control, 20(6).

[15] Liu, B., Zha, Y., Zhang, T. and Chen, S., 2016, May. Fuzzy logic control of dual active bridge in solid state transformer applications. In 2016 Tsinghua University-IET Electrical Engineering Academic Forum (pp. 1-4). IET.

[16] Wu, Y., Mahmud, M.H., Zhao, Y. and Mantooth, H.A., 2020. Uncertainty and disturbance estimator-based robust tracking control for dual-active-bridge converters. IEEE Transactions on Transportation Electrification, 6(4), pp.1791-1800.

[17] Ali, M., Yaqoob, M., Cao, L. and Loo, K.H., 2018. Disturbance-observer-based DC-bus voltage control for ripple mitigation and improved dynamic response in two-stage single-phase inverter system. IEEE Transactions on Industrial Electronics, 66(9), pp.6836-6845.

[18] Ko, P.J. and Tsai, M.C., 2018. H_∞ Control Design of PID-Like Controller for Speed Drive Systems. IEEE Access, 6, pp.36711-36722.

[19] Xu, X., Bao, G., Wang, Y. and Li, Q., 2023. Design of H∞ Robust Controller with Load-Current Feedforward for Dual-Active-Bridge DC–DC Converters Considering Parameters Uncertainty. IEEE Access, 11, pp.72332-72342.

[20] Ren, H. and Ma, L., 2021, July. H-infinity mixed sensitivity control of dual active bridge DC-DC converter. In 2021 IEEE International Conference on Power, Intelligent Computing and Systems (ICPICS) (pp. 16-20). IEEE.

[21] Yang, H. and Yang, L., 2022, February. Model reference adaptive control strategy for dual active bridge converter with improved reference model. In 2022 International Conference on Power Energy Systems and Applications (ICoPESA) (pp. 298-303). IEEE.

[22] Effah, E.K., Effah, F.B., Okyere, P.Y. and Anto, E.K., 2025. Robust adaptive control of dual active bridge DC-DC converter with constant power loading. Power Electronics and Drives, 10, pp.60-73.

[23] Farooq, Z., Zaman, T., Khan, M.A., Muyeen, S.M. and Ibeas, A., 2019. Artificial neural network based adaptive control of single phase dual active bridge with finite time disturbance compensation. IEEE Access, 7, pp.112229-112239.

[24] Dòria-Cerezo, A., Serra, F.M., Esteban, F.D., Biel, D. and Griñó, R., 2022. Comparison of first-and second-order sliding-mode controllers for a dc-dc dual active bridge. IEEE access, 10, pp.40264-40272.

[25] Wang, X., Wang, D., Sun, G., Ni, Y., Song, K. and Li, Y., 2023. A robust voltage control of dual active full bridge converter based on RBF neural network sliding mode control with reduced order modeling approach. Frontiers in Energy Research, 11, p.1225269.

[26] Tiwary, N., Panda, A.K., Narendra, A. and Lenka, R.K., 2022. A robust voltage control of DAB converter with super-twisting sliding mode approach. IEEE Journal of Emerging and Selected Topics in Industrial Electronics, 4(1), pp.288-298.

[27] Sami, I., Ullah, S., Rahman, L.U. and Al-Ismail, F.S., 2025. Advanced third-order super-twisting sliding mode control for enhanced control of grid-connected wind energy systems. Energy Reports, 13, pp.3165-3180.

[28] Shao, S., Chen, L., Shan, Z., Gao, F., Chen, H., Sha, D. and Dragičević, T., 2021. Modeling and advanced control of dual-active-bridge DC–DC converters: A review. IEEE Transactions on Power Electronics, 37(2), pp.1524-1547.

C O P E
Member since 2012
JM08090

This journal is a member of, and subscribes to the principles of,
the Committee on Publication Ethics (COPE).
https://publicationethics.org/members/international-journal-computers-communications-and-control

Cite this paper as:

Anwar, M.A.; Li, W.; Balas, M.; Gu, J.; Asad, M.U.; Abbas, G.; Farooq, U. (2026). Robust Integrated Control for Dual Active Bridge Converters in Aircraft Power System, *International Journal of Computers Communications* & *Control*, 21(5), 7652, 2026.
https://doi.org/10.15837/ijccc.2026.5.7652